Theoretical Study on the Electronic Structure and Optical Properties of Mercury-Containing Diethynylfluorene Monomer, Oligomer, and Polymer

Yi Liao,[†,§] Ji-Kang Feng,*[,†,‡] Li Yang,[†] Ai-Min Ren,[†] and Hong-Xing Zhang[†]

State Key Laboratory of Theoretical and Computational Chemistry, Institute of Theoretical Chemistry, Jilin University, Changchun 130023, People's Republic of China, The College of Chemistry, Jilin University, Changchun 130023, People's Republic of China, and Institute of Functional Material Chemistry, Faculty of Chemistry, Northeast Normal University, Changchun 130024, People's Republic of China

Received July 24, 2004

We present a first-principles study of the structural, electronic, and optical properties on mercury-containing diethynylfluorene monomer, oligomer, and polymer. The aim of our quantum-chemical calculations is to shed light on the role of the transition metal centers in the organometallic system in terms of electronic structure and to estimate the influence of metal on the optical properties of the mercury polyyne polymer as well as the nature of luminescence in the polymer. The results indicate that there is a weak electronic interaction between the metal-based fragment and the π-conjugated organic segments, and consequently the photophysical properties are mainly based on the diethynylfluorene π-conjugated fragment (TFT) with little contribution from the metal center. The role of the metal center can be described as weak delocalization coupled with strong localization characteristics along the organometallic polymer backbone. The lowest singlet and triplet excited state have been studied by the singles configuration interaction (CIS) method and time-dependent density functional method (TDDFT). Comparison of the CIS optimized excited state structure and the Hartree−Fock ground state structure indicates that the geometric shift is mainly confined within one repeat unit in polymer. This strongly localized character of the excited state is illustrated by a frontier orbital contour plot and explained as the effect of the heavy metal, which forms some barrier to delocalization along the conjugated chain. Both singlet and triplet excited states of the polymer are localized mainly on the conjugated ligand segment. Through the chain length dependence of emission energies, we extrapolated an emission peak at 384.9 nm in the polymer, which is comparable to 382 nm observed experimentally for solution phase photoluminescence.

Introduction

There is rapidly growing interest in the study and design of conjugated organometallic complexes and polymers due to their potential applications in electronic and optoelectronic devices such as lasers, photocells, and light-emitting diodes (LEDs).[1] In this respect, rigid-rod metal acetylide materials have attracted the attention of a number of research groups.[2] In earlier work on metal polyynes, a vast range of platinum(II) and gold(II)-containing monomers and polymers have been prepared where alkynyl units are separated by a variety of aromatic ring systems (phenyl, pyridyl, oligothienyl etc.) with different electronic properties.[3] Recently much effort has been devoted by Wong and others in employing fluorene-based spacers to making luminescent bimetallic and organometallic polyyne materials,[4] where the fluorene moiety provides a rigidly planarized biphenyl structure within the polymer backbone as well as

* Corresponding author. E-mail: JiKangf@yahoo.com; Fax: +86-431-8945942.

† State Key Laboratory of Theoretical and Computational Chemistry, Jilin University.

‡ The College of Chemistry, Jilin University.

§ Institute of Functional Material Chemistry, Northeast Normal University.

(1) Heeger, A. J. *Angew. Chem., Int. Ed.* **2001**, *40*, 2591−2611. (b) Stoner, T. C.; Dallinger, R. F.; Hopkins, M. D. *J. Am. Chem. Soc*. **1990**, *112*, 5651−5653. (c) Kokil, A.; Shiyanovskaya, I.; Singer, K.; Weder, C. *J. Am. Chem. Soc*. **2002**, *124*, 9978. (d) Ferri, A.; Polzonetti, G.; Licoccia, S.; Paolesse, R.; Favretto, D.; Traldi, P.; Russo, M. V. *J. Chem. Soc., Dalton Trans.* **1998**, *23*, 4063.

(2) (a) Bruce, D. W.; O'Hare, D. *Inorganic Materials,* 2nd ed.; Wiley: Chichester, U.K., 1996. (b) Long, N. J.; Williams, C. K. *Angew. Chem., Int. Ed*. **2003**, *42*, 2586. (c) Nast, R. *Coord. Chem. Rev*. **1982**, *47*, 89. (d) Nguyen, P.; Gómez-Elipe, P.; Manners, L. *Chem. Rev*. **1999**, *99*, 1515. (e) Younus, M.; Köhler, A.; Cron, S.; Chawdhury, N.; Al-Mandhary, M. R. A.; Khan, M. S.; Lewis, J.; Long, N. J.; Friend, R. H.; Raithby, P. R. *Angew. Chem., Int. Ed*. **1998**, *37*, 3036. (f) Mayr, A.; Yu, M. P. Y. Y.; Yam, V. W. W. *J. Am. Chem. Soc*. **1999**, *121*, 1760. (g) Wong, W. Y.; Wong, C. K.; Lu, G. L. *J. Organomet. Chem*. **2003**, *671*, 27.

(3) (a) Chawdhury, N.; Köhler, A.; Friend, R. H.; Wong, W. Y.; Lewis, J.; Younus, M.; Raithby, P. R.; Corcoran, T. V.; Al-Mandhary, M. R. A.; Khan, M. S. *J. Chem. Phys*. **1999**, *110*, 4963. (b) Chawdhury, N.; Köhler, A.; Friend, R. H.; Younus, M.; Long, N. J.; Raithby, P. R.; Lewis, J. *Macromolecules* **1998**, *31*, 722. (c) Lewis, J.; Long, N. J.; Raithby, P. R.; Shields, G. P.; Wong, W. Y.; Younus, M. *J. Chem. Soc., Dalton Trans*. **1997**, *22*, 4283. (d) Li, P.; Ahrens, B.; Choi, K. H.; Khan, M. S.; Raithby, P. R.; Wilson, P. J.; Wong, W. Y. *CrystEngComm*. **2002**, *4*, 405. (e) Irwin, M. J.; Vittal, J. J.; Puddephatt, R. J. *Organometallics* **1997**, *16*, 3541. (f) Khan, M. S.; Al-Mandhary, M. R. A.; Al-Suti, M. K.; Hisham, A. K.; Raithby, P. R.; Ahrens, B.; Mahon, M. F.; Male, L.; Marseglia, E. A.; Tedesco, E.; Friend, R. H.; Köhler, A.; Feeder N.; Teat, S. J. *J. Chem. Soc., Dalton Trans*. **2002**, *7*, 1358.

10.1021/om0494317 CCC: $30.25
Publication on Web 12/24/2004

the possibility of remote functionalization at the C-9 position. Wong and Liu report first examples of well-defined rigid-rod mercury(II) polyynes with a 9,9-dialkylfluorene spacer (Hg-TFT)$_\infty$,[5] which are highly soluble in common organic solvents such as chloroform and dichloromethane. This is a prerequisite to fabricate organic light-emitting diodes (OLEDs) by the spin-coating method.

To our knowledge, few experimental investigations have been performed on the structure−property relationship of mercury-based polyynes.[6] Experimental measurement, in conjunction with molecular orbital theory, is a valuable tool in analyzing the electronic structure of polymers because it allows an estimate not only of the relative energies of the electronic levels but also of their detailed distribution over the molecule. In recent years, the theoretical methods of quantum-chemistry have provided significant insight into the electronic and optical properties of conjugated polymers.[7] We can reveal the molecular electronic structure of the ground and lowest excited state as well as the nature of absorption and photoluminescence through quantum calculation. For commercial exploitation of this kind of rigid-rod metal polyyne and for direct application-aimed synthesis, a thorough understanding of the relationship between electronic structure and optical property is necessary. It seemed an attractive goal for us to perform detailed theoretical investigation on d^{10} mercury polyynes with fluorenyl linkers.

The majority of the studies on polymers using quantum-chemistry methods consider, in fact, oligomers. The general strategy is the simulation of a number of oligomers of increasing length such that the properties of the polymers can be inferred by extrapolating the results.[8] In this paper we have performed Hartree−Fock (HF) and density functional theory (DFT) calculations on a series of ground-state mercury diethynylfluorene oligomers (Hg-TFT)$_n$ (n = 1−3) as well as their free ligand (TFT)$_n$ (n = 1−3). Given the intrinsic role that excited-state formation plays in the basic photophysics of conjugated polymers and further in their technological applications such as organic light-emitting diodes, the excited state properties may be as significant as or of greater significance than the ground state properties of these systems. Thus, it is of considerable significance to characterize the excited states of model systems. Comparison of the results obtained from these calculations should allow us to obtain useful information concerning the influence on the electronic structure and lowest excitations of incorporating metal atoms along the conjugated path. Moreover, the chain length dependence of the transition energies was also taken into consideration to estimate the spatial conjugation of the lowest singlet and triplet excited state.

Computational Methods

Calculations on electronic ground states described in this paper were performed at the ab initio HF and DFT levels of theory as implemented within the Gaussian 03 software package.[9] Recent studies show that density functional theory calculations are remarkably successful in predicting a wide variety of problems in organometallic chemistry.[10] Becke's three-parameter hybrid method[11] using the Lee−Yang−Parr correlation functional[12] was employed (denoted as B3LYP) here. Gradient optimizations were carried out using the 6-31G* basis set[13] for C and H atoms. Owing to the large number of electrons and to account for relativistic effects, two basis sets with inner electrons substituted by effective core potentials (ECP) were employed for Hg. The first basis set was LanL2DZ, which uses an ECP for inner electrons and double-ζ quality valence functions for the heavier elements.[14] The second basis set employs the ECP60MWB pseudopotential of the Stuttgart/Bonn group.[15] This yields two suites of basis sets used in

(4) (a) Wong, W. Y.; Lam, H. Y.; Lee, S. M. *J. Organomet. Chem*. **2000**, *595*, 70. (b) Wong, W. Y.; Choi, K. H.; Lu, G. L.; Shi, J. X. *Macromol. Rapid Commun*. **2001**, *22*, 461. (c) Khan, M. S.; Al-Mandhary, M. R. A.; Al-Suti, M. K.; Ahrens, B.; Mahon, M. F.; Male, L.; Raithby, P. R.; Boothby, C. E.; Köhler, A. *J. Chem. Soc., Dalton Trans*. **2003**, *1*, 74. (d) Wong, W. Y.; Lu, G. L.; Choi, K. H.; Lin, Z. *Eur. J. Org. Chem*. **2003**, 365. (e) Lewis, J.; Raithby, P. R.; Wong, W. Y. *J. Organomet. Chem*. **1998**, *556*, 219. (f) Wong, W. Y.; Lu, G. L.; Choi, K. H.; Shi, J. X. *Macromolecules* **2002**, *35*, 3506.

(5) Wong, W. Y.; Liu, L.; Shi, J. X. *Angew. Chem., Int. Ed*. **2003**, *42*, 4064.

(6) (a) Wong, W. Y.; Choi, K. H.; Lu, G. L. *Organometallics* **2002**, *20*, 4475. (b) Wong, W. Y.; Choi, K. H.; Lu, G. L.; Shi, J. X.; Lai, P. Y.; Chan, S. M. *Organometallics* **2001**, *20*, 5446. (c) Mingos, D. M. P.; Vilar, R.; Rais, D. *J. Organomet. Chem*. **2002**, *641*, 126.

(7) (a) Brédas, J. L. *Adv. Mater*. **1995**, *7*, 263. (b) Brédas, J. L.; Cornil, J.; Beljonne, D.; Dos Santos, D. A.; Shuai, Z. *Acc. Chem. Res.* **1999**, *32*, 267−276. (c) Ambrosch-Draxl, C.; Majewski, J. A.; Vogl, P.; Leising, G. *Phys. Rev. B* **1995**, *51*, 9668−9676. (d) Cornil, J.; Beljonne D.; Brédas, J. L. In *Electronic Materials: The Oligomer Approach*; Müllen, K., Wegner, G., Eds.; Wiley-VCH: Weinheim, 1998; pp 432−447. (e) Cornil, J., Beljonne D.; Brédas, J. L. In *Electronic Materials: The Oligomer Approach*; Müllen, K., Wegner, G., Eds.; Wiley-VCH: Weinheim, Germany, 1998. (f) Beljonne, D.; Shuai, Z.; Cornil, J.; dos Santos, D. A.; Brédas, J. L. *J. Chem. Phys*. **1999**, *111*, 2829−2841. (g) Hong, S. Y.; Marynick, D. S. *Macromolecules* **1992**, *25*, 4652. (h) De Oliveira, M. A.; Duarte, H.; Pernaut, J.; De Almeida, W. B. *J. Phys. Chem. A* **2000**, *104*, 8256. (i) Brocks, G.; Kelly, P. J. *Synth. Met*. **1993**, *55*−*57*, 4243.

(8) (a) Lahti, P. M.; Obrzut, J.; Karasz, F. E. *Macromolecules* **1987**, *20*, 2023. (b) Forni, A.; Sironi, M.; Raimondi, M.; Cooper, D. L.; Gerratt, J. *J. Phys. Chem. A* **1997**, *101*, 4437. (c) Duke C. B.; Paton, A. In *Conductive Polymers*; Seymour, R. B., Ed.; Plenum: New York, 1981; p 155. (d) Salzner, U.; Lagowski, J. B.; Pickup, P. G.; Poirier, R. A. *Synth. Met*. **1998**, *96*, 177−189. (e) Ford, W. K.; Duke, C. B.; Paton, A. *J. Chem. Phys*. **1982**, *77*, 4564.

(9) Frisch, M. J.; Trucks, G. W.; Schlegel, H. B.; Scuseria, G. E.; Robb, M. A.; Cheeseman, J. R.; Montgomery, J. A., Jr.; Vreven, T.; Kudin, K. N.; Burant, J. C.; Millam, J. M.; Iyengar, S. S.; Tomasi, J.; Barone, V.; Mennucci, B.; Cossi, M.; Scalmani, G.; Rega, N.; Petersson, G. A.; Nakatsuji, H.; Hada, M.; Ehara, M.; Toyota, K.; Fukuda, R.; Hasegawa, J.; Ishida, M.; Nakajima, T.; Honda, Y.; Kitao, O.; Nakai, H.; Klene, M.; Li, X.; Knox, J. E.; Hratchian, H. P.; Cross, J. B.; Adamo, C.; Jaramillo, J.; Gomperts, R.; Stratmann, R. E.; Yazyev, O.; Austin, A. J.; Cammi, R.; Pomelli, C.; Ochterski, J. W.; Ayala, P. Y.; Morokuma, K.; Voth, G. A.; Salvador, P.; Dannenberg, J. J.; Zakrzewski, V. G.; Dapprich, S.; Daniels, A. D.; Strain, M. C.; Farkas, O.; Malick, D. K.; Rabuck, A. D.; Raghavachari, K.; Foresman, J. B.; Ortiz, J. V.; Cui, Q.; Baboul, A. G.; Clifford, S.; Cioslowski, J.; Stefanov, B. B.; Liu, G.; Liashenko, A.; Piskorz, P.; Komaromi, I.; Martin, R. L.; Fox, D. J.; Keith, T.; Al-Laham, M. A.; Peng, C. Y.; Nanayakkara, A.; Challacombe, M.; Gill, P. M. W.; Johnson, B.; Chen, W.; Wong, M. W.; Gonzalez, C.; Pople, J. A. *Gaussian 03, Revision B.04*; Gaussian, Inc.: Pittsburgh, PA, 2003.

(10) (a) Ziegler, T. *Chem. Rev*. **1991**, *91*, 651. (b) Niu, S.; Hall, M. B. *Chem. Rev*. **2000**, *100*, 353. (c) Li, S.; Hall, M. B. *Organometallics* **2001**, *20*, 2153. (d) Conner, D.; Jayaprakash, K. N.; Cundari, T. R.; Gunnoe, T. B. *Organometallics* **2004**, *23*, 2724. (e) Urtel, H.; Bikzhanova, G. A.; Grotjahn, D. B.; Hofmann, P. *Organometallics* **2001**, *20*, 3938. (f) Iron, M. A.; Martin, J. M. L.; Van der Boom, M. E. *J. Am. Chem. Soc*. **2003**, *125*, 11702.

(11) (a) Becke, A. D. *J. Chem. Phys*. **1993**, *98*, 5648. (b) Becke, A. D. *Phys. Rev. A* **1988**, *38*, 3089. (c) Becke, A. D. *J. Chem. Phys*. **1993**, *98*, 1372.

(12) (a) Lee, C.; Yang, W.; Parr, R. G. *Phys. Rev. B* **1988**, *37*, 785. (b) Miehlich, B.; Savin, A.; Stoll, H.; Preuss, H. *Chem. Phys. Lett*. **1989**, *157*, 200.

(13) Hariharan, P. C.; Pople, J. A. *Theor. Chim. Acta* **1973**, *28*, 213.

(14) (a) Hay, P. J.; Wadt, W. R. *J. Chem. Phys*. **1985**, *82*, 270. (b) Wadt, W. R.; Hay, P. J. *J. Chem. Phys*. **1985**, *82*, 284. (c) Hay, P. J.; Wadt, W. R. *J. Chem. Phys*. **1985**, *82*, 299.

(15) Andrae, D.; Haeussermann, U.; Dolg, M.; Stoll, H.; Preuss, H. *Theor. Chim. Acta* **1990**, *77*, 123.

calculation, denoted as L2 (LanL2DZ (3s3p3d)/[2s2p2d] basis sets for Hg and 6-31G* for C, H) and E60 (ECP60MWB (8s7p6d)/[6s5p3d] basis sets for Hg and 6-31G* for C, H), respectively.

The structures of the model systems were optimized in the first singlet excited state (S_1) and triplet excited state (T_1) using configuration interaction with all singly excited determinants (CIS).[16] In a few cases the geometry of the T_1 was examined by optimizing the structure at the unrestricted B3LYP level.

On the basis of ground and excited state optimization, a time-dependent density functional theory (TD-DFT) approach[17] was applied to investigate the excited state electronic properties of oligomers $(Hg\text{-}TFT)_n$ ($n = 1-3$) at the B3LYP/E60 level. For comparison and calibration, the free ligand TFT has also been examined at the same level. Applications of TDDFT have become reliable approaches for the theoretical treatment of electronic excitation processes,[18] and recent works demonstrate the good accuracy for a wide range of organometallic systems.[19] TD-B3LYP was utilized by Rillema et al. to interpret the spectroscopic behavior of the monomer, dimer, and trimer of $[Pt(bph)(CO)_2]$ in solution.[19a] Charmant and co-workers[19b] successfully applied TD-DFT for studying the first excited state features of platinum−thallium alkynyl complexes, from which the luminescence is attributed to charge transfer from Tl−Pt unit to the platinum metal fragments. M. D. Halls[19c] and R. L. Martin[19d] have studied the lowest singlet excited states of tris(8-hydroxyquinolate)aluminum (Alq_3) with the TD-B3LYP approach, and the calculated excitation and emission energies were in excellent agreement with the experimental values. Han and Lee[19e] also reported from their systematic calculations on methyl-substituted tris(8-hydroxyquinolate)aluminum ($Almq_3$) that the TD-B3LYP method provided the most reliable results for the transition energies. All the calculations described here were performed at the SGI Origin 2000 server.

Results and Discussion

The properties of the polymer depend greatly on their constituent monomer and oligomers. Here, we choose mercury monomer (that will form the repeated unit of the polymer under consideration) and oligomer $(Hg\text{-}TFT)_n$ ($n = 1-3$) as model systems (shown in Figure 1). To reveal the nature of bonding between the metal center and diethynylflurene, oligo(2,7-diethynylflurene) $(TFT)_n$ ($n = 1-3$) were also taken into consideration (see Figure 1). It should be pointed out that the dioctal substitution at C-9 in the fluorine ring existing in polymer $(Hg\text{-}TFT)_\infty$ offers the prospect of improved polymer processing and mediating potential interchain interactions in films.[20] While this remote substitution at C-9 produces less impact on the electronic structure of the conjugated backbone, as confirmed by comparison of frontier molecular orbitals between Hg-TFT and its 9,9-dioctal-substituted derivative (see Supporting Information). Considering the trivial influence of the side chain on the electronic structure of the polymer, we replace it with an H atom for simple calculation. In fact, it is common in theoretical calculations to use hydrogen to substitute the alkyl side chain far from the polymer backbone for simplicity.

Ground State Geometry. In Table 1 crystallographic data are compared to selected optimized structures of $(Hg\text{-}TFT)_1$ at B3LYP/L2 and B3LYP/E60 levels of theory. Table 1 shows that in our calculation with the small Lanl2dz basis set for mercury the bond lengths of Hg−CC and Hg−CH_3 are overestimated by 0.11 and 0.12 Å, respectively. Employing a larger basis set, ECP60MWB, for mercury results in significantly more accurate bond lengths, whose mean structural deviations fall well within 0.014 Å. Therefore, treating 5s and 5p electrons in addition to traditional 5d, 6s electrons explicitly in the calculations is significant in description bonding of Hg acetylide, and we adopt this basis set for Hg in oligomer $(Hg\text{-}TFT)_n$ calculations hereafter.

The optimized structure of $(Hg\text{-}TFT)_1$ exhibits nearly planar geometry (the angles C−Hg−C, C≡C−Hg, and C−C≡C are close to 180°), which is in agreement with the X-ray measurement, where the bimercury centers adopt a two-coordinate linear geometry in a rigid-rod manner. However, there are no experimental values for the conformation of mercury polyyne or oligomers. In the absence of structural information, we have assumed the oligomers to be planar because of two reasons: (i) interchain interactions (packing force) tend to significantly reduce the torsion angles between adjacent units in the solid state (as is the case of oligophenylenes[21a] and neutral hexapyrrole[21b]) (ii) electronic and optical properties are weakly affected by small changes in torsional angels.[22] To determine the minimum energy configuration as well as energy differences between the cis- and trans-conformation, we perform fully geometrical optimizations on $(Hg\text{-}TFT)_n$ ($n = 2-4$) with B3LYP/E60. The results show both trans- and cis-conformations are local minima and the trans-conformation is only slightly more stable than the cis one, by about 0.02−0.04 kcal/mol. In view of the steric hindrance from the 9,9-dioctal substituent on the polymer backbone, cis- and trans-alkyl-substituted $(Hg\text{-}TFT)_4$ are

(16) (a) Foresman, J. B.; Head-Gordon, M.; Pople, J. A.; Frisch, M. J. *J. Phys. Chem*. **1992**, *96*, 135. (b) Foresman, J. B.; Frisch, A. E. *Exploring Chemistry with Electronic Structure Methods*, 2nd ed.; Gaussian Inc.: Pittsburgh, PA, 1995; Chapter 8, p 213. (c) van Gisbergen, S. J. A.; Groeneveld, J. A.; Rosa, A.; Snijders, J. G.; Baerends, E. J. *J. Phys. Chem. A* **1999**, *103*, 6835.

(17) (a) Casida, M. K.; Jamorski, C.; Casida, K. C.; Salahub, D. R. *J. Chem. Phys*. **1998**, *108*, 4439. (b) Stratmann, R. E.; Scuseria, G. E. *J. Chem. Phys*. **1998**, *109*, 8218.

(18) (a) Casida, M. E. In *Recent Advances in Density Functional Methods*; Chong, D. P., Ed.; World Scientific: Singapore, 1995; Part I, p 155. (b) Casida, M. E. In *Accurate Description of Low-Lying Molecular States and Potential Energy Surfaces*; Hoffmann, M. R., Dyall, K. G., Ed.; American Chemical Society: Washington, D.C., 2002; p 199. (c) Daniel, C. *Coord. Chem. Rev*. **2003**, *238−239*, 143. (d) Rosa, A.; Baerends, E. J.; vanGisbergen, S. J. A.; vanLenthe, E.; Gooeneveld, J. A.; Snijders, J. G. *J. Am. Chem. Soc*. **1999**, *121*, 10356. (e) Adamo, C.; Barone, V. *Theor. Chem. Acc*. **2000**, *105*, 169. (f) Boulet, P.; Chermett, H.; Daul, C.; Gilardoni, F.; Rogemond, F.; Weber, J.; Zuber, G. *J. Phys. Chem. A* **2001**, *105*, 885. (g) Farrell, I. R.; van Slageren, J.; Zalis, S.; Vlcek, A. *Inorg. Chim. Acta* **2001**, *315*, 44.

(19) (a) Stoyanov, S. R.; Villegas, J. M.; Rillema, D. P. *Inorg. Chem*. **2003**, *42*, 7852. (b) Charmant, J. P. H.; Forniés, J.; Gómez, J.; Lalinde, E.; Merino, R. I.; Moreno, M. T.; Orpen, A. G. *Organometallics* **2003**, *22*, 652. (c) Halls, M. D.; Schlegel, H. B. *Chem. Mater*. **2001**, *13*, 2632. (d) Martin, R. L.; Kress, J. D.; Campbell, I. H. *Phys. Rev. B* **2000**, *61*, 15804. (e) Han, Y. K.; Lee, S. U. *Chem. Phys. Lett*. **2002**, *366*, 9.

(20) (a) Scherf, U.; List, E. J. *Adv. Mater*. **2002**, *14*, 477. (b) Jenekhe S. A.; Osaheni, J. A. *Science* **1994**, *265*, 765. (c) Kraft, A.; Grimsdale A. C.; Holmes, A. B. *Angew. Chem., Int. Ed*. **1998**, *37*, 402. (d) Yu, W.-L.; Pei, J.; Cao, Y.; Huang W.; Heeger, A. J. *Chem. Commun*. **1999**, *1837*. (e) Lemmer, U.; Hein, S.; Mahrt, R. F.; Scherf, U.; Hopmeir, M.; Wiegner, U.; Göbel, R. O.; Müllen, K.; Bässler, H. *Chem. Phys. Lett*. **1995**, *240*, 371.

(21) (a) Puschnig, P.; Ambrosch-Draxl, C. *Phys. Rev. B* **1999**, *60*, 7891. (b) Colle, R.; Curioni, A. *J. Phys. Chem. A* **2000**, *104*, 8546−8550.

(22) Brédas, J. L.; Silbey, R.; Boudreaux, D. S.; Chance, R. R. *J. Am. Chem. Soc*. **1983**, *22*, 6555.

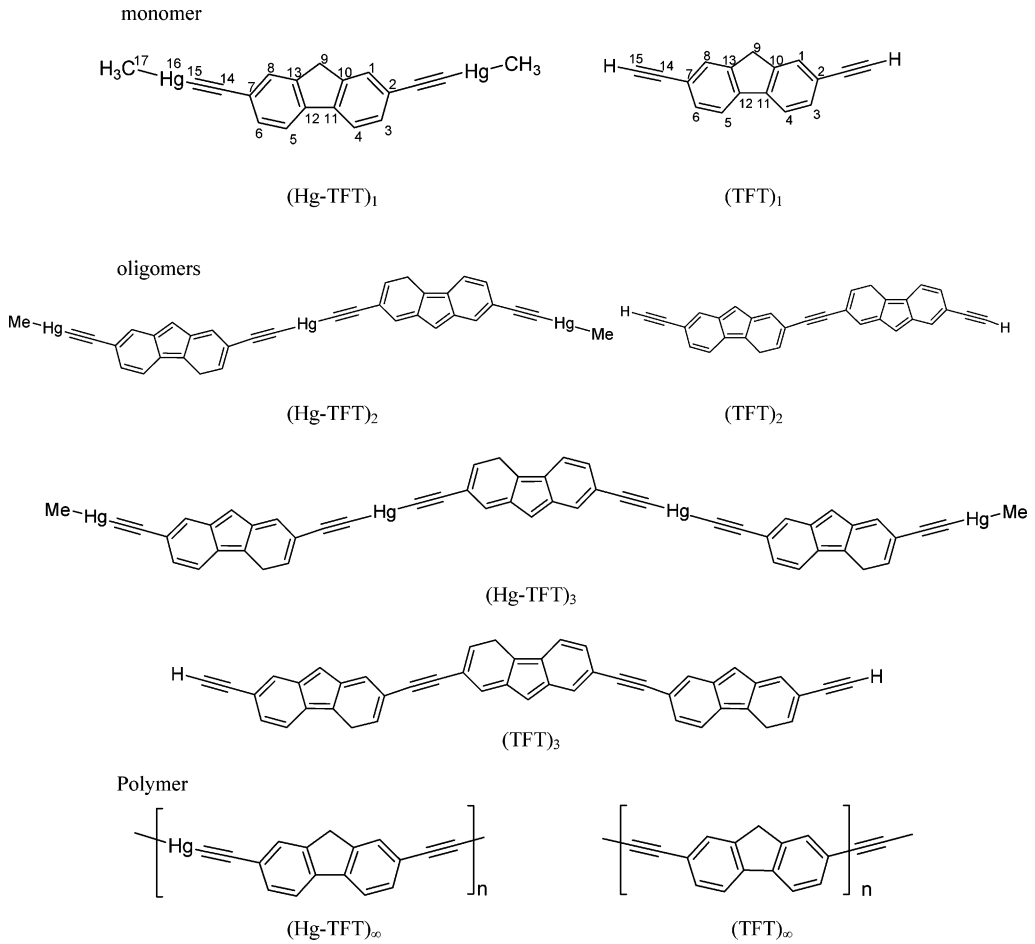

Figure 1. Structures of the polymer and monomers that have been investigated, together with the abbreviations that are used for them. The triple bonds are abbreviated by T, and fluorene rings by F. Monomers and polymers are differentiated by use of the subscripts 1 and ∞, respectively.

Table 1. Comparison of Calculated and Experimental Structural Data for (Hg-TFT)$_1$

		C≡C (Å)	Hg−CC (Å)	Hg−CH_3 (Å)	C−Hg−C (deg)	C≡C−Hg (deg)	C−C≡C (deg)
calc	L2	1.225	2.158	2.205	179.96	179.74	179.97
	E60	1.224	2.046	2.096	179.93	179.94	179.93
expt[a]		1.209(13)	2.045(8)	2.080(11)	177.75	176.87	178.78

[a] Experimental data from ref 5.

investigated with the ONIOM method[23] using B3LYP/Genecp (ECP60MWB for Hg; 3-21G* for C and H) for the core and HF/Genecp (ECP60MWB for Hg; sto-3G for C and H) for the alkyl-substituted sections of the molecule. This time the energy difference between trans- and cis-conformations increases apparently by up to 0.56 kcal/mol. Both structures have similar bond lengths, whereas the topology is quite different, as is illustrated in Figure 2. It can be noted that only the chain of the trans-configuration extends along the *z* axis, while the chain of the cis-configuration exhibits a curvature due to the steric effects. Recently, several oligo(fluorene)s' derivatives with trans-conformation were synthesized and characterized.[24] Among these trans-oligomers, the

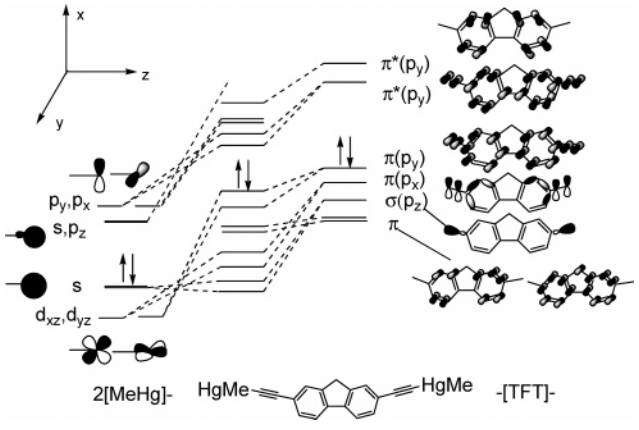

Figure 2. Interaction diagram showing the main contributions to the LUMO, HOMO, *n*HOMO, and *n*LUMO in Hg-TFT.

alkyl-substituted fluorene polyyne reported by Bunz et al.[24c] most resembles our title system. In fact, many polymers and oligomers were considered as anti-conformation in quantum-chemical calculations.[25] On

(23) (a) Svensson, M.; Humbel, S.; Froese, R. D. J.; Matsubara, T.; Sieber, S.; Morokuma, K. J. *J. Phys. Chem.* **1996**, *100*, 19357. (b) Humbel, S.; Sieber, S.; Morokuma, K. J. *J. Chem. Phys.* **1996**, *105*, 1959.

(24) (a) Culligan, S. W.; Geng, Y.; Chen, S. H.; Klubek, K.; Vaeth, K. M.; Tang, C. W. *Adv. Mater.* **2003**, *15*, 1176. (b) Mastrorilli, P.; Nobile, C. F.; Grisorio, R.; Rizzuti, A.; Suranna, G. P.; Acierno, D.; Amendola, E.; Iannelli, P. *Macromolecules* **2004**, *37*, 4488. (c) Pschirer, N. G.; Bunz, U. H. F. *Macromolecules* **2000**, *33*, 3961.

Table 2. Optimized Bond Lengths (Å) of $(TFT)_n$ and $(Hg\text{-}TFT)_n$ ($n = 1-3$) with B3LYP/E60

	$(TFT)_1$	$(TFT)_2$	$(TFT)_3$	$(Hg\text{-}TFT)_1$	$(Hg\text{-}TFT)_2$	$(Hg\text{-}TFT)_3$
C_1-C_2	1.411	1.414	1.414	1.413	1.413	1.413
C_3-C_4	1.391	1.391	1.390	1.392	1.391	1.391
C_4-C_{11}	1.398	1.398	1.398	1.399	1.399	1.399
$C_{10}-C_{11}$	1.412	1.412	1.413	1.413	1.413	1.413
$C_{11}-C_{12}$	1.465	1.464	1.463	1.465	1.464	1.464
C_9-C_{10}	1.516	1.516	1.516	1.516	1.516	1.516
C_7-C_{14}	1.428	1.428[a]	1.428[a]	1.427	1.427[a]	1.427[a]
		1.422[b]	1.422[b]		1.426[b]	1.426[b]
C≡C	1.210	1.211[a]	1.211[a]	1.224	1.224[a]	1.224[a]
		1.218[b]	1.218[b]		1.223[b]	1.223[b]
Hg−CC				2.046	2.046[a]	2.046[a]
					2.010[b]	2.010[b]
$Hg-CH_3$				2.098	2.097	2.097

[a] Bond lies in the terminal chain. [b] Inter-ring bond between neighboring repeat fluorene rings.

Table 3. Molecular Orbital Components of Hg-TFT (%) at the B3LYP/E60 Level

orbital no.	composition of MO						
89	π^*p_y (fluorene) (92%)						
88			p_x (C≡C) (14%)	+	p_x (Hg) (74%)		
87			p_x (C≡C) (14%)	+	p_x (Hg) (73%)		
86	π^*p_y (fluorene) (21%)	+	πp_y (C≡C) (15%)	+	p_y (Hg) (60%)		
85(LUMO)	π^*p_y (fluorene) (67%)	+	πp_y (C≡C) (15%)	+	p_y (Hg) (17%)		
84(HOMO)	πp_y (fluorene) (70%)	+	πp_y (C≡C) (26%)	+	d_{yz} (Hg) (4%)		
83	πp_y (fluorene) (41%)	+	πp_y (C≡C) (54%)	+	d_{yz} (Hg) (5%)		
82	πp_y (fluorene) (100%)						
81	πp_y (fluorene) (100%)						
80	σ(fluorene) (17%)	+	πp_x (C≡C) (77%)	+	d_{xz} (Hg) (6.4%)		
79	σ(fluorene) (14%)	+	πp_x (C≡C) (79%)	+	d_{xz} (Hg) (6.5%)		
78			σp_z (C≡C) (24%)	+	S, p_z (Hg) (32%)	+	p_z (CH_3) (39%)
77			σp_z (C≡C) (24%)	+	S, p_z (Hg) (32%)	+	p_z (CH_3) (39%)

the basis of the above analyses we choose the energetically favorable trans-configuration in the following calculations. Meanwhile, work is in progress to investigate the optoelectronic properties of mercury polyyne with cis-conformation and subsequently compare them with corresponding trans isomer.

The stable structures of oligomers $(Hg\text{-}TFT)_n$ are calculated and compared with their conjugated segments $(TFT)_n$ ($n = 1-3$). Table 2 presents only the variation of calculated bond length with the number of repeat units n in the series of conjugated $(Hg\text{-}TFT)_n$ and $(TFT)_n$ ($n = 1-3$) because the bond angles and dihedrals are nearly invariable.

It can be seen that the geometries change little with increasing chain length in $(Hg\text{-}TFT)_n$ and $(TFT)_n$. The average bond length deviation is less than 0.003 Å in both series, especially for series $(Hg\text{-}TFT)_n$. All the parameters remained nearly unchanged (<0.001 Å) on going from $(Hg\text{-}TFT)_1$, to $(Hg\text{-}TFT)_2$, to $(Hg\text{-}TFT)_3$. This suggests that polymerization has little effect on the geometrical structure of repeat unit Hg-TFT, and we can describe the basic structures of the polymers as their monomers. The only discrepancy between monomer and polymer is that there exists a new kind of bridging segment linking two adjacent fluorene segments in the polymers. For example, in $(TFT)_2$ we have inter-ring C≡C (1.218 Å) labeled with superscript b slightly larger than C≡C (1.211 Å) in the terminal chain labeled with superscript a; in $(Hg\text{-}TFT)_2$ and $(Hg\text{-}TFT)_3$, the inter-ring bond length, 2.010 Å, between Hg and the alkynyl carbon is smaller than the average 2.046 Å Hg−C(acetylene) bond lying in the chain end. This is probably to be expected since the inter-ring atom Hg connected by two alkynyl carbons would accumulate more positive charge than that in the chain end, which results in a more polarized Hg−CC bond.

Comparing geometrical data between $(TFT)_n$ and $(Hg\text{-}TFT)_n$, one may find that coordination of the metal Hg exerts little effect on the structure of the fluorene ring, where the mean deviation is lowers less than 0.002 Å and change mainly occurs on the alkynyl bridge. For instance, the C≡C bond length increases from 1.218 Å in $(TFT)_3$ to 1.223 Å in $(Hg\text{-}TFT)_3$. This is the result of coordination between the metal center and the alkynyl carbon and may be indicative of a possible weak elongation in conjugation through the metal center.

Electronic Structure. Rationalizing the nature of the metal−carbon bond in mercury acetylide is crucial for interpreting their photophysical properties and is a logical prerequisite for the design of electronic materials composed of metal−alkynyl building blocks.

A fragment calculation shows the main interactions between the diethynylfluorene-based fragment −[C≡C−F−C≡C]− (−[TFT]−) and the methyl mercury center [MeHg]− in Hg-TFT with the conjugated structure lying in the *xz* plane and the chain-axis oriented along *z* (see Figure 2). For clarity, the contribution of each component to a MO is also calculated besides assignment of the composition of the MO on the basis of fragment calculation. Table 3 shows frontier molecular orbital components of Hg-TFT.

It can be seen that in Hg-TFT frontier occupied MOs (nHOMOs) concentrate mainly on the fluorene ring or alkynyl fragment or both of them, with little contribution from the d orbital of metal center. For example, the first two orbitals in Hg-TFT consist mainly of π

(25) (a) Ehrendorfer Ch.; Karpfen, A. *J. Phys. Chem.* **1994**, *98*, 7492. (b) Stafström, S.; Brédas, J. L. *Phys. Rev. B* **1988**, *38*, 4180. (c) Bakhshi, A. K.; Ladik, J. *Int. J. Quantum Chem.* **1992**, *42*, 997. (d) Zojer, E.; Pogantsch, A.; Hennebicq, E.; Beljonne, D.; Brédas, J. L.; de Freitas, P. S.; Scherf, U.; List, E. J. W. *J. Chem. Phys.* **2002**, *117*, 6794−6802.

orbitals of the ligand −[C≡C−F−C≡C]− (∼95%) and a few metal d_{yz} orbital components (∼5%), followed by two orbitals containing completely $\pi(p_y)$ of the fluorene ring in the ligand fragment. On the contrary, improved contribution from the metal p orbital can be found in frontier virtual MOs (*n*LUMOs). For instance, the lowest unoccupied orbital (LUMO) is a π^* orbital with atomic orbital contributions of 67% from the fluorene ring, 15% from acetylene, and 17% from the p_y component from mercury; as for the LUMO+1, Hg p_y composition increases to 60%. From these analyses, intraligand excitation (IL) accompanied by little ligand−metal charge transfer (LMCT) was expected during excitation.

The main bonding of an acetylide ligand to a transition metal center is well established and best described in terms of overlap of the sp-hybridized σ orbital of the [C≡CR]− fragment with a metal fragment orbital of similar symmetry. Here interaction between the s,p_z-hybridized orbital of Hg and the acetylene p_z orbital forming a stable Hg−C σ bond was found in lower orbitals 77 and 78. These orbitals are localized in nature and construct a molecule framework. They will not participate in low-lying optical excitation due to their low energy level, while the π-type interaction provides a pathway for delocalization of electron density between the metal and ligand and, hence, is crucial for optoelectronic process. In this system, weak $p\pi-d\pi$ interactions between the ligand and the metal result in weak delocalization along the molecule chain. This picture is consistent with previous analysis that the HOMO contained considerable ligand π character and little metal π component. This metal $d\pi$ manifold is closer in energy to the filled ligand π orbitals than to their antibonding counterparts. Therefore, the acetylide acts as a π donor ligand rather than as a π acceptor.

Another important characteristic of the electronic structure that we are interested in is the energy gap between the HOMO and LUMO. The MO calculation and fragment analysis showed that the energy gap decreased by 0.31 eV from the free ligand TFT to the complex Hg-TFT, and metal fragment affects the HOMO more than the LUMO. This can be explained as weak delocalization through the metal center and ligand TFT. As a consequence, the first optically allowed excitation, corresponding essentially to a HOMO−LUMO transition (see next section), is red shifted with respect to the corresponding transition in the free ligand TFT.

To gain greater insight into this weak delocalization, it is worthwhile to compare the energy levels of $(TFT)_n$ and $(Hg\text{-}TFT)_n$ ($n = 1-3$) (shown in Figure 3).

From the schematic representation of the energy levels in Figure 3, we can find that with an increase in chain length both series show decreasing energy gap, as illustrated by the convergent red line. The energy difference between the HOMO and LUMO is 4.16, 3.46, and 3.21 eV on going from TFT to $(TFT)_2$ and to $(TFT)_3$, which can be attributed to the extension in conjugation. In the case of oligomer $(Hg\text{-}TFT)_n$, the energy gap decreases by 0.21 eV when going from (Hg-TFT) (3.85 eV) to $(Hg\text{-}TFT)_2$ (3.64 eV) and then to a lesser extent of 0.08 eV upon further increasing the chain length to $(Hg\text{-}TFT)_3$ (3.56 eV). It is clear that the energy gap decreases at a higher rate in $(TFT)_n$ than in $(Hg\text{-}TFT)_n$, which can be explained as larger conjugation and

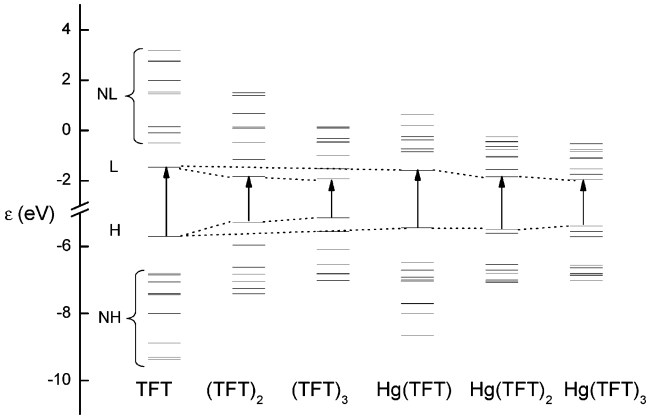

Figure 3. Schematic drawing of the energies of NHOMO (NH), HOMO (H), LUMO (L), and NLUMO (NL) orbitals for $(TFT)_n$ and $Hg(TFT)_n$ ($n = 1-3$).

π-electron delocalization along the $(TFT)_n$ chain and relatively weaker conjugation along the corresponding $(Hg\text{-}TFT)_n$ chain.

Photoexcited and Photoluminescent Processes. In the present study, time-dependent density functional theory is employed to study the characters and vertical excitation energies of low-lying excited states of oligomers $(Hg\text{-}TFT)_n$.

1. Excitation Energy. Table 4 presents calculated excitation energies and excitation characteristics of selected excited states with greater oscillator strengths (above 0.5). Compared with the available experimental excitation wavelength (ca. 358 nm) for Hg-TFT in thin solid films (11 K),[5] the deviation of the calculated values is merely 7 nm, confirming that TDDFT with the B3LYP functional can give relatively accurate predictions on vertical excitation energies for this series of systems.

The linearity between the calculated excitation energies and the reciprocal chain length is excellent for oligomer $(Hg\text{-}TFT)_n$ (see Table 4). By extrapolating the resultant linear relationship to infinite chain length, the excitation energy of the corresponding polymer can be predicted. Moreover, the effective conjugated length (ECL) can also be evaluated. The ECL may be defined as the minimum number of repeat units to produce saturation of the optoelectronic properties; thus the information on the ELC of the polymers is very useful for determining such important electronic properties as band gaps, absorption coefficients, etc. It is often possible to determine the limiting conjugation length of oligomeric materials by examination of the plot of maximum absorption energy versus reciprocal number of chain length $1/n$, as long as soluble high molecular weight materials are available for comparison.[26] With the limiting absorption maximum of 375 nm determined for high molecular weight mercury polyyne (DP = 24),[5] linear extrapolation of the plot in Figure 4 would suggest an effective conjugation length of approximately four repeat units in mercury polyyne. This extended length is markedly lower than the average ECL of 10 repeat units for the polyfluorene ethynylene derivatives reported by Lee et al.[27] It can be explained in that the

(26) (a) Schenk, R.; Ehrenfreund, M.; Huber, W.; Müllen, K. *J. Chem. Soc., Chem. Commun*. **1990**, 1673. (b) Kohler, B. K. *Springer Ser. Solid State Sci*. **1985**, *63*, 101. (c) Tolbert, L. M. *Acc. Chem. Res*. **1992**, *25*, 561.

(27) Lee, S. H.; Nakamura, T.; Tsutsui, T. *Org. Lett*. **2001**, *3*, 2005.

Table 4. Selected Calculated Excitation Energies (*E*), Wavelengths (*λ*), Oscillator Strenghs (×c4), and Dominant Excitation Character for Low-Lying Singlet (S_n) States of Oligomers $(Hg\text{-}TFT)_n$[a]

oligomers	state	composition		ΔE (eV)/λ (nm)	expt	×a6	character
TFT	1	H→L	64%	3.96/313		1.04	IL
(Hg-TFT)1	1	H→L	65%	3.53/351	358	1.61	IL + LMCT
(Hg-TFT)2	1	H→L	67%	3.40/365		2.57	IL + LMCT
	5	H-1→L+1	67%	3.90/318		1.22	IL + LMCT
(Hg-TFT)3	1	H→L	64%	3.35/371		3.69	IL + LMCT
		H-1→L+1	17%				
	5	H-1→L+1	62%	3.71/335	345	0.72	IL + LMCT
		H→L	16%				
$(Hg\text{-}TFT)_\infty$				3.27/379	364		

[a] For comparison TFT is also listed. H denotes the HOMO and L the LUMO. Experimental data from ref 5.

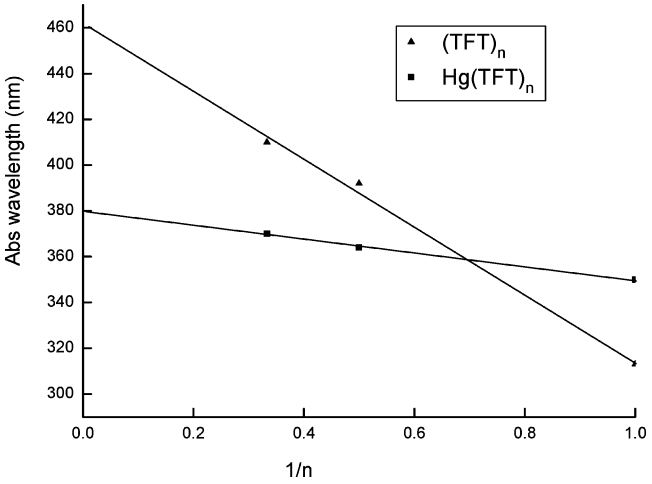

Figure 4. Excitation energy calculated with TD-B3LYP as a function of $1/n$ in oligomers $(Hg\text{-}TFT)_n$ and $(TFT)_n$.

heavy metal forms some barrier to delocalization along the conjugated chain, though weak π conjugation was found to be preserved through the metal atom due to weak interaction between the metal fragment and the dialkynylfluorene fragment.

As can be seen from Figure 4, the plot using the data points obtained for the oligomers is reasonably linear (correlation coefficient = 0.998 for mercury series). However, linear extrapolation to $1/n = 0$ yields a value of 379 nm for mercury polyyne excitation energy and 462 nm for alkynyl polyfluorene. As one can see, this prediction underestimates the excitation energy of polymer $(Hg\text{-}TFT)_\infty$ by 15 nm. Three factors may be responsible for the error. One is that calculations on a few longer oligomers may be required so that more data could be used in the linear regression. Another is that the predicted excitation energy is for the isolated gas phase chain, while the experimental one is measured in the condensed phase, where interchain interactions may be contributing. Additionally, simple calculation models were adopted, which differ from real polymers.

We can also see from Figure 4 that the slope of mercury oligomers is apparently lower than that of purely organic ligands. This suggests a less pronounced red-shift absorption in $(Hg\text{-}TFT)_n$ than in $(TFT)_n$ as the chain length increases, which points again to the weaker conjugation of $(Hg\text{-}TFT)_n$ than $(TFT)_n$ as stated above.

Photophysiscal investigations of the excited state properties of Hg-TFT and its analogues have been undertaken experimentally.[6b] Inspection of the absorption and emission spectra from metal alkynyl (M-TRT, M = Au, Pt, Hg) in solvated and condensed phase systems shows that they all display similar spectral shape. These similar spectral patterns are suggestive of the ligand-dominating excited state. The same trend can be observed in our theoretical calculation. In Table 4, The lowest energy singlet transition ($S_0 \rightarrow S_1$) for oligomers $(Hg\text{-}TFT)_n$ at the DFT level of theory has the greatest oscillator strength (*f*) and is mainly transition HOMO → LUMO in character. As shown in Figure 5, the HOMOs are all π orbitals of the diethynylfluorene ligand with little contribution from the metal center and LUMOs are π^* orbitals localized mainly on the dialkynylfluorene lignd with improving metal fragment component. For each oligomer, their corresponding orbitals are very similar in terms of appearance and resemble those of free ligand TFT. This lowest energy transition ($S_0 \rightarrow S_1$) is assigned as the 0−0 absorption peak in UV spectra and mainly intraligand (IL) $\pi\pi^*$ transition mixing with little ligand-to-metal charge transfer (LMCT). In UV spectra for polymer $(Hg\text{-}TFT)_\infty$, we can also observe a shoulder peak at around 345 nm. We assign this weak absorption as $S_0 \rightarrow S_5$, that is, HOMO−1 → LUMO+1 transition, due to its relative transition energy and oscillator strength.

The lowest energy absorption peak with $S_0 \rightarrow S_1$ transition is found red-shifted in Hg-TFT, as compared to that of the free ligand (TFT). This reveals that the extent of π conjugation is increased when incorporating the metal center in the conjugated fragment. The red shift of the absorption energy can be rationalized by the bonding interaction between metal center and diethynylfluorene fragment, which causes a narrowing of the band gap and thus an extension in π-conjugation. TD-DFT calculations also predict a decreasing red shift of $S_0 \rightarrow S_1$ transition in oligomer $(Hg\text{-}TFT)_n$ as *n* increases and converges to 379 nm at $n = 4$. This indicates that the first optical absorption transition in the polymer $(Hg\text{-}TFT)_\infty$ arising from the promotion of one electron from the HOMO to the LUMO is delocalized over about four repeat units. Examination of the absorption energy on going from (Hg-TFT) to $(Hg\text{-}TFT)_n$ and to $(Hg\text{-}TFT)_\infty$ corroborates that the effect of the metal center is weak delocalization and strong localization.

2. Excited State Structure. Studies of the excited state properties for a number of molecules using the CIS method have found that, despite the tendency of CIS to overestimate electronic transition energies, the excited state potential energy surface can often be quite ac-

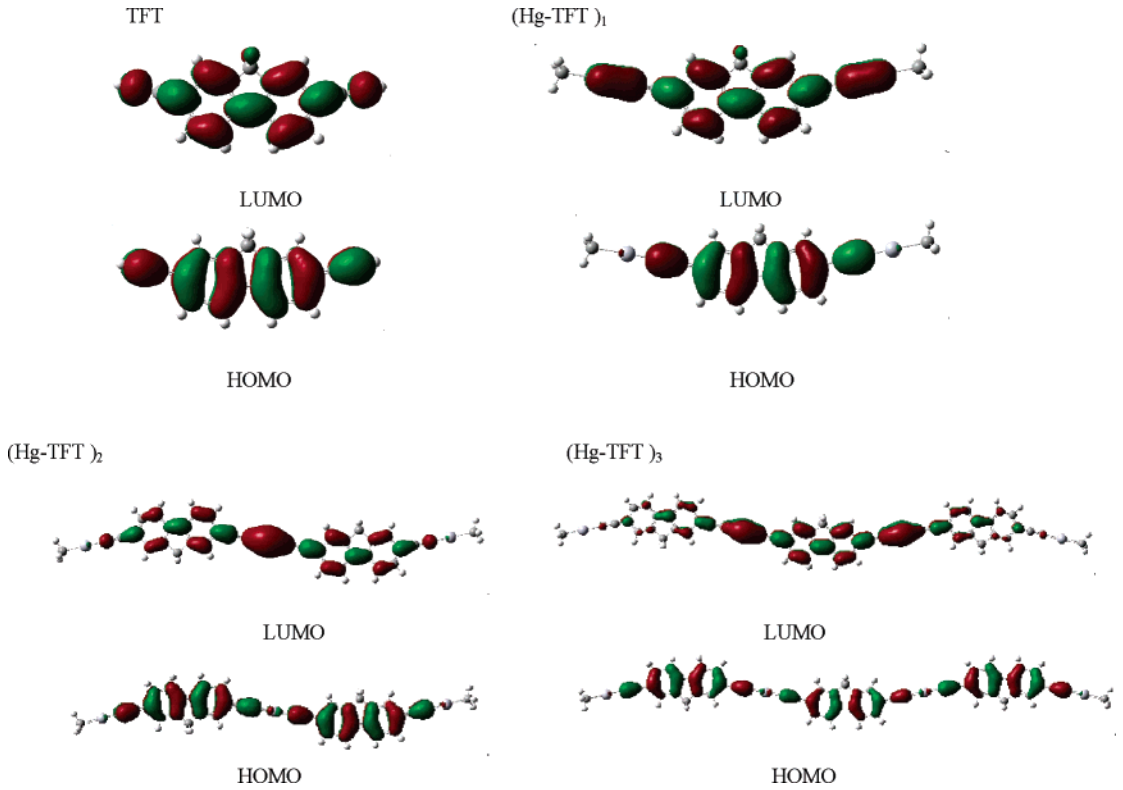

Figure 5. Contour plots of frontier occupied and virtual orbitals involved in low-lying singlet excitation in oligomers $(Hg\text{-}TFT)_n$ ($n = 1-3$). (For comparison TFT is also listed.)

Table 5. HF/E60 Ground State and CIS/E60 Excited State Bond Lengths (Å) for Unit I in $(Hg\text{-}TFT)_1$ and Units I and II in $(Hg\text{-}TFT)_2$ (molecule labeling shown in Figure 1)

						(Hg-TFT)$_2$				
	(Hg-TFT)$_1$					S_0	S_1		T_1	
bond length	S_0	S_1	S_1-S_0	T_1	T_1-S_0	I (II)	I	II	I	II
r(1,2)	1.397	1.421	0.024	1.429	0.032	1.397	1.397	1.421	1.397	1.428
r(2,3)	1.396	1.425	0.029	1.427	0.031	1.396	1.397	1.426	1.396	1.427
r(3,4)	1.383	1.361	−0.022	1.363	−0.020	1.383	1.382	1.361	1.383	1.362
r(4,11)	1.386	1.422	0.036	1.427	0.041	1.386	1.387	1.422	1.386	1.426
r(1,10)	1.378	1.359	−0.019	1.358	−0.020	1.378	1.377	1.359	1.378	1.358
r(10,11)	1.396	1.434	0.038	1.438	0.042	1.396	1.397	1.434	1.396	1.438
r(11,12)	1.471	1.404	−0.067	1.406	−0.065	1.471	1.470	1.405	1.471	1.406
r(9,10)	1.514	1.516	0.002	1.517	0.003	1.514	1.514	1.515	1.514	1.517
r(7,14)	1.440	1.408	−0.032	1.417	−0.023	1.440[a]	1.440[a]	1.410[a]	1.440[a]	1.416[a]
						1.438[b]	1.438[b]	1.407[b]	1.438[b]	1.414[b]
r(14,15)	1.202	1.214	0.012	1.209	0.007	1.202[a]	1.202[a]	1.213[a]	1.202[a]	1.209[a]
						1.201[b]	1.201[b]	1.213[b]	1.201[b]	1.208[b]
r(15,16)	2.066	2.066	0.000	2.066	0.000	2.067[a]	2.066[a]	2.067[a]	2.067[a]	2.066[a]
						2.036[b]	2.034[b]	2.033[b]	2.036[b]	2.034[b]
r(16,17)	2.111	2.112	0.001	2.111	0.000	2.111	2.111	2.111	2.111	2.112

[a] Bond lies in the terminal chain. [b] Inter-ring bond between neighboring repeat fluorene rings.

curate, as evidenced by comparison of equilibrium excited state structure with experiment.[19c,28]

The S1 and T_1 geometries of $(Hg\text{-}TFT)_n$ ($n = 1, 2$) were optimized at the CIS/E60 level of theory to investigate the geometry relaxation associated with electronic excitation to the lowest energy singlet excited state ($S_0 \rightarrow S_1$) and lowest triplet excited state ($S_0 \rightarrow T_1$). For comparison, the HF/E60 ground state bond lengths are also listed in Table 5 with the bond lengths of $(Hg\text{-}TFT)_n$ ($n = 1, 2$) in the S_1 and T_1 states. Note that positive and negative values in the S_1-S_0 and T_1-S_0 columns indicate bond elongation and contraction in the excited state, respectively. Two repeat units of $(Hg\text{-}TFT)_2$ in the excited states lost their uniform structures exhibited in the ground state and were labeled as I and II for differentiation.

a. S_1 and T_1 States of Hg-TFT. With respect to the S_1 and T_1 states of Hg-TFT, the geometry structures have the following two major changes compared with its corresponding HF/E60 ground state (see Table 5). First, pronounced geometrical change is calculated in the diethynylfluorene fragment than in the metal fragment, which appears to be extremely rigid with respect to excitation. Furthermore, more prominent modifica-

(28) (a) Foresman, J. B.; Head-Gordon, M.; Pople, J. A.; Frisch, M. J. *J. Phys. Chem.* **1992**, *96*, 135. (b) Foresman, J. B.; Schlegel, H. B. In *Recent Experimental and Computational Advances in Molecular Spectroscopy*; Gausto, R., Hollas, J. M., Eds.; Kluwer Academic: Dordrecht, The Netherlands, 1993; Vol. 406, p 11. (c) Tirapattur, S.; Belletête, M.; Leclerc, M.; Durocher, G. *J. Mol. Struct. (THEOCHEM)* **2003**, *625*, 141.

Table 6. Calculated Fluorescence ($S_1 \rightarrow S_0$) and Phosphorescence ($T_1 \rightarrow S_0$) Wavelengths (λ) and Their Transition Nature of Oligomers (Hg-TFT)$_n$ (n = 1−3) with Available Experimental Data from Ref 5

	$S_1 \rightarrow S0$					$T_1 \rightarrow S0$			
oligomers	composition		$\Delta E/\lambda$ (nm)	expt	×a6	composition		$\Delta E/\lambda$ (nm)	expt
TFT	H→L	62%	3.63/342		1.10	H→L	79%	2.12/586	
(Hg-TFT)$_1$	H→L	64%	3.25/381	374[b]	1.74	H→L	65%	1.94/640	591*
(Hg-TFT)$_2$	H→L	62%	3.24/383		2.53	H→L	74%	1.93/641	
(Hg-TFT)$_3$	H→L	64%	3.23/384		3.61	H→L	71%	1.93/643	
(Hg-TFT)$_\infty$			3.23/384	382[b]				1.93/643	630*[c] 583[c]

[a] For comparison TFT is also listed. H denotes the HOMO and L the LUMO. Asterisks indicate that emission peaks appear as shoulders. All experimental data are from ref 5. [b] Emission spectra measurement in CH_2Cl_2. [c] Emission spectra (11 K) measured in thin solid films.

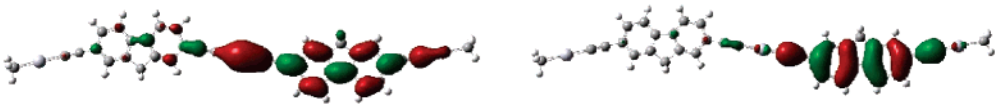

LUMO HOMO

Figure 6. Contour plots of highest occupied and lowest virtual orbitals of (Hg-TFT)$_2$ in the S_1 state.

tions are centralized on the fluorene ring of the diethynylfluorene ligand than in the ethynyl part. Second, enhancement in bond-length alternation leads to the appearance of a quinoid geometric character on the excited states of the fluorene ring. For example, Δr (defined as the difference between the lengths of the C−C bonds orientated obliquely to the chain axis and those oriented along the chain axis, that is $[r(1,2) + r(2,3) + r(4,11) + r(10,11) + r(9,10)]/5 - [r(3,4) + r(1,10) + r(11,12)]/3$) increased from ∼0.007 Å in the ground state to ∼0.068 Å in the singlet excited state and ∼0.073 Å in triplet state. This larger bond length alternation in T_1 relative to S_1 is in accordance with larger relaxation energies in T_1 (0.33 eV) than S_1 (0.29 eV) upon vertical excitation.

The relaxation of the structures during the excitation can also be determined from the character of the nodal patterns of the frontier molecule orbital involved in the excited transition. For example, the lowest energy singlet excitation ($S_0 \rightarrow S_1$) is mainly HOMO → LUMO in character (see Table 4 and Figure 5). The LUMO has nodes across the C_1-C_2, C_2-C_3, C_4-C_{11}, $C_{10}-C_{11}$, C_9-C_{10}, and $C_{14}-C_{15}$ bonds, but the HOMO is bonding in these regions. Therefore one would expect elongation of these bonds. Table 5 shows that these bonds are in fact considerably longer in the excited state and present quinoid character. The HOMO has a node across the C_3-C_4, C_1-C_{10}, $C_{11}-C_{12}$, and C_7-C_{14} bond, while the LUMO is bonding. The data in Table 5 confirm the anticipated contraction of these bonds.

b. S_1 and T_1 States of (Hg-TFT)$_2$. On comparison of the ground and excited state geometries for I and II in (Hg-TFT)$_2$, we can point out the following observations.

(i) The structural shift is predominantly localized on unit II. Unit I in (Hg-TFT)$_2$ is practically unaffected, especially in the T1 state.

(ii) The S_1 geometry of unit II in (Hg-TFT)$_2$ resembles that of (Hg-TFT)$_1$ in the S_1 state. Accordingly, The T_1 geometry of unit II in (Hg-TFT)$_2$ preserves geometrical characteristics from (Hg-TFT)$_1$ in the T_1 state.

These results suggest that the S_1 and T_1 excited states in (Hg-TFT)$_2$ are strongly localized after relaxation and present particular properties of corresponding monomer excited state through the $S_0 \rightarrow S_1$ excitation delocalized over four repeat units. This is not surprising in view of the rigid character of the metal−alkynyl bond during the relaxation (see Table 5, $\Delta r(15,16) \approx 0$ Å from S_0 to S_1 and T_1 state), which may confine the excitons to be more localized but not completely within one repeat unit. Given the close dependence of emission on the nature of the excited state, we may conjecture that the spectral shift of the emission peak from the monomer to polymer is small and the emission process is more localized than the absorption process after relaxation.

3. Emission Energy

At this stage, we would like to discuss the fluorescence ($S_1 \rightarrow S_0$) and phosphoresce ($T_1 \rightarrow S_0$) emission energies of (Hg-TFT)$_n$ employing TDDFT calculation on the basis of CIS optimized excited states. Table 6 presents calculated maximal emission wavelengths in the S_1 and T_1 state for oligomers (Hg-TFT)$_n$ (n = 1−3). For clarity, the frontier orbitals of (Hg-TFT)$_2$ involved in the $S_1 \rightarrow S_0$ transition are depicted as examples in Figure 6. The $T_1 \rightarrow S_0$ transition process is illustrated by frontier orbitals and spin density of (Hg-TFT)$_3$ in the Supporting Information.

As shown in Table 6, the lowest energy emissions of (Hg-TFT)$_n$ (n = 1−3), which are the same as the corresponding absorption, consist mainly of HOMO−LUMO electron promotion. The HOMOs and LUMOs are all π-type orbitals dominated by orbitals originating from the diethynylfluorene fragment in all cases with little contribution from the metal center. Thus the maximal wavelength emission in S_1 and T_1 for (Hg-TFT)$_n$ is $^1(\pi\pi^*)$ and $^3(\pi\pi^*)$ in nature, respectively. The calculated S_1 emission wavelength (381 nm) of (Hg-TFT)$_1$ is in good agreement with the experimental emission peak around 374 nm in dichloromethane. Out results in Table 6 indicate that both singlet and triplet emission energies are nearly unchanged on going from monomer to dimer and to trimer. That is, there is no size dependence of emission energies and the emission process may exhibit localized characteristics in (Hg-TFT)$_\infty$. When the singlet emission energies of (Hg-TFT)$_n$ and (TFT)$_n$ are plotted as a function of the

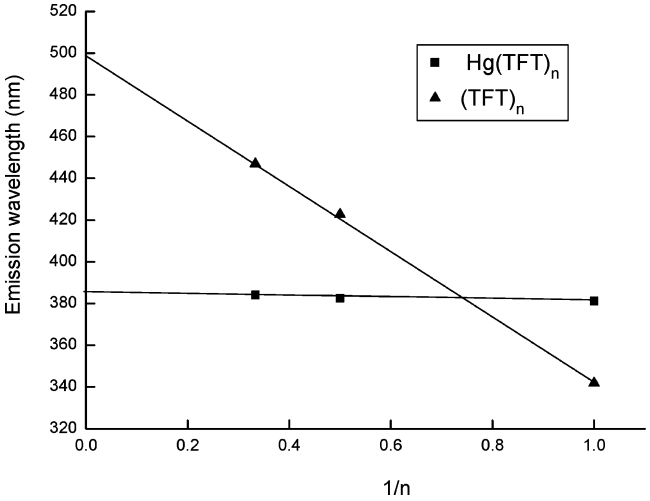

Figure 7. Emission energy of the singlet state calculated with TD-B3LYP as a function of $1/n$ in oligomers $(Hg\text{-}TFT)_n$ and $(TFT)_n$.

reciprocal number of repeat units, $1/n$ (shown in Figure 7), a significant deviating behavior is found between them as expected. The pronounced red shift of emission energies for $(TFT)_n$ from monomer to dimer and to trimer is clearly caused by the strong π conjugation, as is often the case for conjugated organic polymers, while the emission of $(Hg\text{-}TFT)_\infty$ is almost localized. Therefore, by chemical modification of the monomer (Hg-TFT)'s framework, the luminescent properties of the corresponding polymer can be fine-tuned and reasonably predicted on the molecule level. This is an important guideline in experimental synthesis of photovoltaic devices with this kind of material.

In our calculation, the S_1 and T_1 emission energies display insignificant red shift (within 4 nm) from monomer to polymer, unlike the absorption energies. This is consistent with essentially localized singlet and triplet excitons after relaxation discussed above. Generally, the extent or confinement of the excitation depends on the nature of the particular orbitals involved in the respective electronic transition. As illustrated in Figure 6 and Figure 10 (in Supporting Information), the HOMO and LUMO involved in S_1 or T_1 emission are mainly concentrated on one repeat unit, different from the delocalized frontier obitals exhibited in the singlet absorption process in Figure 5. The spin density map for the lowest triplet states of $(Hg\text{-}TFT)_3$ plotted in Figure 10 also presents electrons mainly localized within one repeat unit. All these calculations suggest strongly localized S_1 and T_1 emission states.

The prediction on fluorescence is in excellent agreement with the results of optical emission measurements of polymer in CH_2Cl_2, which show an intense $^1(\pi\pi^*)$ emission peak at 382 nm.[5] However, a discrepancy was found between theoretical calculation and experimental measurement where a greater degree of delocalization in the polymer T_1 state was inferred from the red shift of experimental phosphorescent spectra from monomer to polymer. Without exclusion of the limit of the quantum approach, one possible reason for this difference is that in contrast to gas phase calculations our phosphorescent spectra were measured in the condensed phase, which may result in strong interchain interactions due to aggregate formation,[29] just as Wong pointed out that they cannot rule out the possibility that the red shifts are related to the number and/or strength of the Hg···Hg interactions in the polymers.[5] Through our elaborate excited state calculation, we infer that the red shift from monomer to polymer may be the result of interchain interaction and the excited states should be of a more localized character.

Conclusion

In this work, a first-principles density functional method was employed to study the geometrical and electronic structures of $(Hg\text{-}TFT)_n$ and $(TFT)_n$ ($n = 1-3$). π-Conjugation was preserved through the metal atom due to weak hybridization between the pπ orbital of the conjugated ligand and the Hg dπ orbital. A stronger localized Hg−C σ bond was found between the metal and conjugated ligand. Further electronic spectrum calculations confirm that the introduction of a metal center into the conjugated segments contributes more to confine the excitons than to delocalize the π electrons. TDDFT calculations predict π-conjugation extended over about four repeat units in the polymer $(Hg\text{-}TFT)_\infty$ singlet absorption process and localized mainly on one unit in S_1 and T_1 emission after relaxation. The geometrical change in the polymer singlet and triplet excited states was almost confined within one unit relative to the ground state. The heavy metal atom forms some barrier to delocalization, so that the first singlet and triplet excited states of the polymer have the character of molecular excited states and mainly ligand-dominating excited state. Thus this kind of rigid-rod organometallic polymer can be used as a good emitter layer in displays due to their potential of achieving full color emission through modifying the electronic structure of the conjugated ligand segment. Through our elaborate theoretical investigation, we not only well reproduce the experimental spectra but also reveal the nature and mechanism in luminescence, which provide useful reference to the functional molecular designs based on the transition metal polyyne.

Acknowledgment. This investigation was supported by the Major State Basis Research Development Program (No. 2002CB 613406) and the National Nature Science Foundation of China (No. 90101026 20173021) as well as Youth Science Foundation of Northeast Normal University (111494018).

Supporting Information Available: Contour plot showing frontier molecular orbitals of Hg-TFT and its 9,9-dioctal substituent; the structure of optimized alkyl-substituted $(Hg\text{-}TFT)_4$; contour plots of HOMO and LUMO; and spin density map of $(Hg\text{-}TFT)_3$ in the T_1 state. This material is available free of charge via the Internet at http://pubs.acs.org.

OM0494317

(29) (a) Puddephatt, R. J. *Coord. Chem. Rev*. **2001**, *216−217*, 313. (b) Scherf, U.; Müllen, K. *Makromol. Chem. Rapid Commun.* **1991**, *12*, 489. (c) Grem, G.; Leising, G. *Synth. Met*. **1993**, *57*, 4105. (d) Halkyard, C. E.; Rampey, M. E.; Kloppenburg, L.; Studer-Martinez, S. L.; Bunz, U. H. F. *Macromolecules* **1998**, *31*, 8655−8659.